14th International Symposium on Turbulence and Shear Flow Phenomena (TSFP14)
Heidelberg, Germany, July 28–31, 2026

AN EXACT ANALYTICAL FRAMEWORK FOR SPATIOTEMPORAL MODAL ANALYSIS OF A TURBULENT CHANNEL

Miya C. Y. Coimbra
Department of Mechanical Engineering
Stanford University
Stanford, CA 94305, USA
coimbra@stanford.edu

Beverley J. McKeon
Department of Mechanical Engineering
Stanford University
Stanford, CA 94305, USA
bjmckeon@stanford.edu

ABSTRACT

We develop an exact analytical framework for spatiotemporal modal analysis of turbulent channel flow. The aperiodicity in the temporal signal is discussed and an appropriate spatiotemporal mode is estimated, which retains the analytically derived conservation properties that hold for exact spatial modes. Spatiotemporal modal analysis enables the recovery of wall-normal information that is typically obscured in purely spatial modal analyses. This reintroduction provides a more complete picture of turbulent flow dynamics, capturing the nonlinear energy transfer across spectral scales and also its variation across the channel height in physical space. We show that this spatiotemporal framework restricts the spatial arrangement of triadically resonant modes within the channel. The conservation properties of resonant modes are used to study mode-to-mode energy transfer and we discuss how this framework provides the capability to elucidate the specific roles of known coherent structures in the energy transfer process. In particular, we select a representative mode to emulate a very-large-scale motion (VLSM) and determine its role in energy transfer and how it varies with interactions that occur at different wall-normal locations.

INTRODUCTION

The nonlinear term in the Navier-Stokes equations is a primary source of the challenges that come with modeling and predicting the nature of turbulent flows. Modal representations of turbulent velocity fields enable the analysis of this nonlinearity in terms of triadic interactions, providing some structure in the interpretation of the chaotic system. It is known that triadically resonant spatial modes (defined by spatial Fourier transforms) are globally energy conserving, and it has also been shown that spatially triadic interactions are conservative on a triad-by-triad basis. Kraichnan (1957) first noted this in homogeneous isotropic turbulence and it was later shown to apply to wall-bounded flows as well (Schmid and Henningson, 2002); both analyses were carried out in the temporal domain. This conservation property has been utilized in prior contributions to study temporally and/or spatially averaged mode-by-mode energy transfer, see e.g. Cho *et al*. (2018), Ding *et al*. (2025), and Domaradzki *et al*. (1994). Barthel (2022) showed that exact spatiotemporal modes, which have a temporal frequency wavenumber component, are also energy conserving on a triad-by-triad basis. While spatial modes are exact in a channel flow due to periodic boundary conditions, exact temporal modes cannot be defined because of the non-periodic nature of the temporal signal. In this study, the wall-normal information is reintroduced by estimating and incorporating the temporal frequency component of a spatiotemporal mode into the analysis. We analytically demonstrate that the estimated spatiotemporal modes satisfy mode-by-mode energy conservation exactly, enabling the use of spatiotemporal triadic interactions to study energy transfer in turbulent channel flow.

ANALYTICAL DEVELOPMENT OF SPATIOTEMPORAL MODES

We consider a channel flow with periodic boundary conditions in the streamwise (x) and spanwise (z) directions. The spatial Fourier transforms in these periodic directions result in exact spatial Fourier modes, $\hat{u}_j(\boldsymbol{k},y,t)$. The spatial wavenumber is $\boldsymbol{k}=[k_x,k_z]$ and y is the wall-normal coordinate. Spatiotemporal modes require an additional Fourier transform of the temporal signal, which is aperiodic in a turbulent flow (this is addressed in a later section). First, let an exact spatiotemporal Fourier mode be defined as $\tilde{\hat{u}}_j(\tilde{\boldsymbol{k}},y)=\mathscr{F}_t[\hat{u}_j(\boldsymbol{k},y,t)]$, where $\tilde{\boldsymbol{k}}=[k_x,k_z,\omega]$. The turbulent kinetic energy (TKE) equation for an exact spatiotemporal mode is then given by

$$\Re\left[\tilde{\hat{u}}^*(\tilde{\boldsymbol{k}},y)\tilde{\hat{v}}(\tilde{\boldsymbol{k}},y)\frac{dU}{dy}\right]+\Re\left[\frac{\partial}{\partial y}\left(\tilde{\hat{v}}^*(\tilde{\boldsymbol{k}},y)\tilde{\hat{p}}(\tilde{\boldsymbol{k}},y)\right)\right] \tag{1}$$
$$+\frac{1}{Re_\tau}\left[2k^2E(\tilde{\boldsymbol{k}},y)-\frac{\partial^2E(\tilde{\boldsymbol{k}},y)}{\partial y^2}+\frac{\partial\tilde{\hat{u}}_j^*(\tilde{\boldsymbol{k}},y)}{\partial y}\frac{\partial\tilde{\hat{u}}_j(\tilde{\boldsymbol{k}},y)}{\partial y}\right]$$
$$=-\Re\left[\mathscr{T}(\tilde{\boldsymbol{k}},y)\right]$$

where

$$\mathscr{T}(\tilde{\boldsymbol{k}},y) = \tilde{\hat{u}}_j^*(\tilde{\boldsymbol{k}},y)\sum_{\tilde{\boldsymbol{k}}'}\tilde{\hat{u}}_m(\tilde{\boldsymbol{k}}',y)\frac{\partial}{\partial x_m}\tilde{\hat{u}}_j(\tilde{\boldsymbol{k}}'',y) \tag{2}$$

is the nonlinear energy transfer term. It is apparent from (2) that only modes that satisfy $\tilde{\boldsymbol{k}} = \tilde{\boldsymbol{k}}' + \tilde{\boldsymbol{k}}''$ contribute to $\mathscr{T}(\tilde{\boldsymbol{k}},y)$. As a result, the resonance condition for a spatiotemporal mode requires triadic compatibility on the k_x, k_z, and ω wavenumber components simultaneously.

It can be shown that energy is conserved within a single triadic set, i.e. when $\tilde{\boldsymbol{k}}$ and $\tilde{\boldsymbol{k}}'$ are fixed. Consider

$$\mathscr{S}(\tilde{\boldsymbol{k}},\tilde{\boldsymbol{k}}',\tilde{\boldsymbol{k}}'') = \int_{-1}^{1}\tilde{\hat{u}}_j^*(\tilde{\boldsymbol{k}},y)\tilde{\hat{u}}_m(\tilde{\boldsymbol{k}}',y)\frac{\partial}{\partial x_m}\tilde{\hat{u}}_j(\tilde{\boldsymbol{k}}'',y)dy, \tag{3}$$

which describes the energy transferred to $\tilde{\boldsymbol{k}}$ via $\tilde{\boldsymbol{k}}'$ from $\tilde{\boldsymbol{k}}''$. The net transfer to $\tilde{\boldsymbol{k}}$ from this fixed triad is then the sum of the energy transferred to $\tilde{\boldsymbol{k}}$ from $\tilde{\boldsymbol{k}}'$ and $\tilde{\boldsymbol{k}}''$

$$\mathscr{N}_{\tilde{\boldsymbol{k}}} = \mathscr{S}(\tilde{\boldsymbol{k}},\tilde{\boldsymbol{k}}',\tilde{\boldsymbol{k}}'') + \mathscr{S}(\tilde{\boldsymbol{k}},\tilde{\boldsymbol{k}}'',\tilde{\boldsymbol{k}}'). \tag{4}$$

Then, triad-by-triad energy conservation states that $\mathscr{N}_{\tilde{\boldsymbol{k}}} + \mathscr{N}_{\tilde{\boldsymbol{k}}'} + \mathscr{N}_{\tilde{\boldsymbol{k}}''} = 0$ (shown in Barthel (2022) and Coimbra and McKeon (2025) for channel flows).

Addressing temporal aperiodicity

To address the non-periodic nature of the temporal signal of a turbulent flow we apply a Hann window, $w(t)$, onto the time-dependent spatially transformed modes to enforce periodicity and extract valid spatiotemporal modes. The windowed spatiotemporal mode is defined as

$$\tilde{\hat{h}}_j(\tilde{\boldsymbol{k}},y) = \mathscr{F}_t[w(t)\hat{u}_j(\boldsymbol{k},y,t)]. \tag{5}$$

We note that while $\tilde{\hat{h}}_j$ is not equivalent to the "exact" spatiotemporal mode associated with the original velocity signal, since the Hann window is a single-tone signal with only three non-zero coefficients, the mode $\tilde{\hat{h}}_j(\tilde{\boldsymbol{k}}_m,y)$ is a weighted sum of $\tilde{\hat{u}}_j(\tilde{\boldsymbol{k}}_{m-1},y)$, $\tilde{\hat{u}}_j(\tilde{\boldsymbol{k}}_m,y)$ and $\tilde{\hat{u}}_j(\tilde{\boldsymbol{k}}_{m+1},y)$ and can be considered a valid approximation for modes of the original signal.

Consider a triadic set of windowed resonant modes where the energy transferred to $\tilde{\boldsymbol{k}}$ via $\tilde{\boldsymbol{k}}'$ from $\tilde{\boldsymbol{k}}''$ is

$$S(\tilde{\boldsymbol{k}},\tilde{\boldsymbol{k}}',\tilde{\boldsymbol{k}}'') = \int_{-1}^{1}\tilde{\hat{h}}_j^*(\tilde{\boldsymbol{k}},y)\tilde{\hat{h}}_m(\tilde{\boldsymbol{k}}',y)\frac{\partial}{\partial x_m}\tilde{\hat{h}}_j(\tilde{\boldsymbol{k}}'',y)dy \tag{6}$$

as defined in (3) but with $\tilde{\hat{h}}_j(\tilde{\boldsymbol{k}},y)$ replacing $\tilde{\hat{u}}_j(\tilde{\boldsymbol{k}},y)$. Critically, the windowing operation is applied to the temporal signal and leaves the spatial signal unaffected. This allows for the estimated spatiotemporal modes to exactly retain triad-by-triad energy conservation; the energy conservation property arises from resonance on the spatial wavenumbers, due to the spatial derivative in the nonlinear term (eq. 2). As a result, we can write $N_{\tilde{\boldsymbol{k}}} + N_{\tilde{\boldsymbol{k}}'} + N_{\tilde{\boldsymbol{k}}''} = 0$, where

$$N_{\tilde{\boldsymbol{k}}} = S(\tilde{\boldsymbol{k}},\tilde{\boldsymbol{k}}',\tilde{\boldsymbol{k}}'') + S(\tilde{\boldsymbol{k}},\tilde{\boldsymbol{k}}'',\tilde{\boldsymbol{k}}'), \tag{7}$$

as is similarly defined in eq. 4.

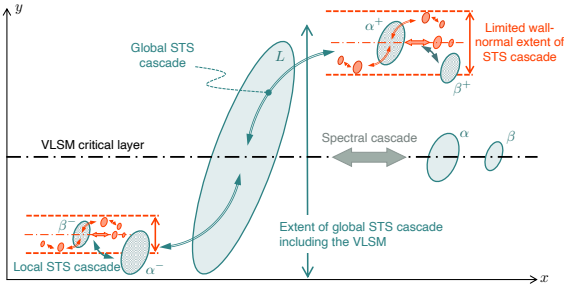

Figure 1. The wall-normal architecture of resonant triads in the spatiotemporal-spectral (STS) framework. The two small scales must both be below the largest scale in the triad, shown by the triad (L,α^-,β^-) or both above the largest scale, as in (L,α^+,β^+). The larger of the two small-scales, α^+ or α^- must have a critical layer further from L than their β counterparts. The only exception is when α and β share the same critical layer as L, shown by (L,α,β). Energy transfer pathways associated with both spectral and spatial transfer of energy are denoted by the global and local STS pathways. A purely spectral cascade has no associated spatial transport of energy.

Spatial Arrangement of Resonant Spatiotemporal Modes

Spatiotemporal modal representations allow us to utilize a mode's critical layer to index a corresponding wall-normal location for each mode. The frequency component of the wavenumber vector can be written as $\omega = ck_x$, where c is the mode wave speed that defines its critical layer. We refer to the mode's location as that of its critical layer (McKeon and Sharma, 2010), which is defined as $y_c = \{y : \overline{U}(y) = c\}$, where $\overline{U}(y)$ is the mean velocity profile. The significance of the critical layer is derived from stability theory (Schmid and Henningson, 2001) and its connection to a mode's location has been utilized in previous studies, e.g. Jacobi *et al.* (2021).

For the remainder of this paper, modes in a resonant triad will be referred to as L,α, and β, with wavenumbers $\tilde{\boldsymbol{k}}_L,\tilde{\boldsymbol{k}}_\alpha$ and $\tilde{\boldsymbol{k}}_\beta$ satisfying $\tilde{\boldsymbol{k}}_L = \tilde{\boldsymbol{k}}_\alpha + \tilde{\boldsymbol{k}}_\beta$. We take $|k_{xL}| < |k_{x\alpha}| < |k_{x\beta}|$, which can be done without any loss of generality. Resonance on the frequency component can be written out as $\omega_L = \omega_\alpha + \omega_\beta$ or $c_L k_{xL} = c_\alpha k_{x\alpha} + c_\beta k_{x\beta}$. Using this triadic resonance condition on ω and adhering to the wavenumber convection for L,α, and β, we discuss two results for the relative critical layer locations of modes in a resonant triad (details in Coimbra and McKeon (2024)). First, the two smaller (in physical space) modes (α,β) cannot straddle the critical layer of L, i.e. the small-scale modes must reside on the same side of its critical layer, y_{cL}. Thus, resonant triads with critical layers below that of L (shown as α^- and β^- in Fig. 1) can at most transport energy up to y_{cL} within that triadic interaction. In order for energy from the triad (L,α^-,β^-) to cross above y_{cL}, L must interact with two modes above it, such as (L,α^+,β^+) in Fig. 1. Then, among interactions resonant with L, its critical layer serves as a physical separation across which energy can only be transferred through two separate interactions with L. Second, the β modes (i.e. the mode with the larger k_x component) must sit closer to the critical layer of L, as shown in Fig. 1. This reveals a symmetry in the arrangement of scales relative to the large-scale critical layer, but a non-monotonic spatial arrangement relative to the wall: below the critical layer, the larger mode is closer to the wall and above it the smaller mode is closer. We note that the symmetry that arises in this spatiotemporal-spectral (STS) structure can

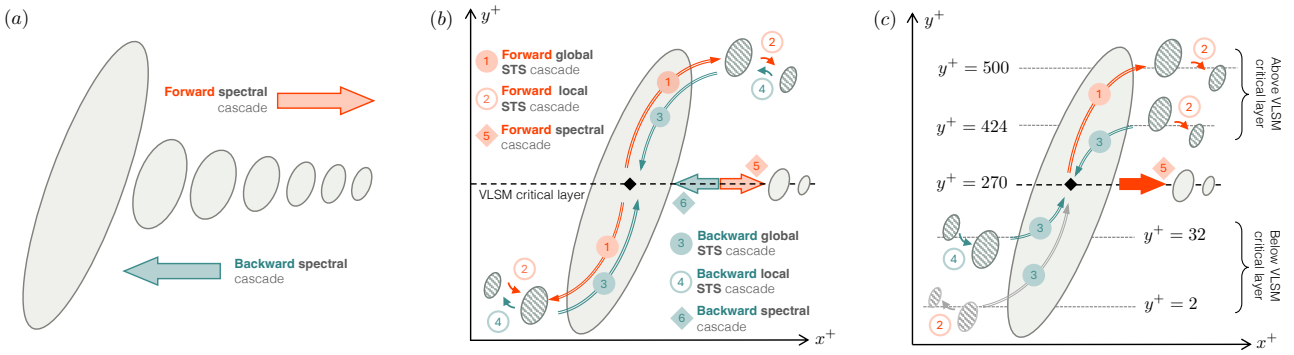

Figure 2. (a) The classical description of the energy cascade, which describes only spectral transfer of energy. The orange arrow denotes the sense of the forward cascade, where energy is transferred from large to small scales, and the blue arrow denotes the sense of the backwards cascade. (b) All energy transfer pathways admitted by the STS framework. Orange arrows denote the sense of the forward cascades and blue arrows denote backward cascades. The double-lined arrows illustrate the larger wall-normal extent of the global STS cascades (numbered 1 and 3) and the single lined arrows denote the local STS cascade (numbered 2 and 4). When all three modes share the same critical layer, the STS framework describes a purely spectral cascade (numbered 5 and 6). (c) The senses of the global and local STS cascades observed in a single temporal segment from interactions with small-scales with critical layers at $y^+ = 2, 43, 424$, and 500. The sense of the purely spectral cascade among triads at the same critical layer is also shown at $y^+ = 270$. Blue arrows denote a backwards cascade and orange arrows denote a forward cascade.

be applied to any triad; the STS structure is shown for blue triads, but also the triads that use α^+ and β^- as the large scales, shown in orange in Fig. 1.

SPATIOTEMPORAL-SPECTRAL ENERGY CASCADE

We combine our understanding of the constrained spatial arrangement and the exact energy conservation properties of the temporally windowed spatiotemporal modes to identify the sense of energy transfer in both the spatial (y) and spectral domains. This formulation is also used to examine the role of large-scale coherent structures in transferring energy across the physical and spectral domains on a mode-by-mode basis.

We consider a single large-scale structure for this analysis, i.e. a spatiotemporal mode that could be thought of as a representative very-large-scale motion (VLSM). We will refer to this representative mode as L, with wavenumber $\tilde{\boldsymbol{k}}_L$, throughout. Additionally, we consider modes with $c \geq 0$, as there is very little energy associated with modes that have negative wave speeds. In computing the energy transfer to some mode $\tilde{\boldsymbol{k}}$, we consider the energy transferred to all modes attributed to the same physical scale, i.e. all negative and conjugate wavenumber pairs needed to describe a real signal. For example, if $\tilde{\boldsymbol{k}} = [k_x, k_z, ck_x]$, we consider the energy transferred to the set $(\tilde{\boldsymbol{k}}, \tilde{\boldsymbol{k}}^*, -\tilde{\boldsymbol{k}}, -\tilde{\boldsymbol{k}}^*)$, where $\tilde{\boldsymbol{k}}^* \equiv [k_x, -k_z, ck_x]$. This describes the energy transferred to a mode of that physical scale, as would be realized in physical space.

Wall-normal transport in the STS cascade

The classical description of the energy cascade, shown in Fig. 2(a), has the capability of describing forward and backward spectral transfer, but there is no information regarding energy transport in the inhomogeneous direction(s). The spatiotemporal framework expands the classical description of the turbulence cascade to capture the spatial (in the wall-normal direction) transport of energy that accompanies the spectral transfer. The possible pathways for this spatiotemporal-spectral (STS) cascade are shown in Fig. 2(b). The orange and blue arrows denote forward and backward transfers of energy, respectively. A forward cascade is typically understood to be energy transfer from larger to smaller scales. Additionally, by expanding the nonlinear energy transfer term on the right-hand-side of eq. 1 and computing the individual transfer terms for each mode in an energy-exchanging triad, i.e. eq. 6, we can define "global" and "local" STS cascades. The global cascades (numbers 1 and 3 in Fig. 2(b) describe the energy transfer from L to the wall-normal region of α and β in the triad. We refer to this cascade as "global" since it has the potential for transferring energy over long distances in y, particularly for L with a large wall-normal extent, as is characteristic of VLSMs. The "local" STS cascades (numbers 2 and 4) describe the energy transfer between the two small-scales in the triad. The critical layers of the small-scale modes are closer to each other in the wall-normal sense, and if L is very large, meaning its wavenumbers are small, the two small-scale modes are also local in spectral space. When all three modes in the triad share the same critical layer, the STS framework describes a purely spectral cascade (numbers 5 and 6). Since all modes share the same critical layer, there is no wall-normal transport associated with the spectral cascade in this case.

We compute the energy transfer among windowed spatiotemporal triads resonant with a representative large scale $\tilde{\boldsymbol{k}}_L = [1, 7, 0.9146]$, which has an aspect ratio consistent with a VLSM-like structure. The data was obtained from a direct numerical simulation of channel flow at $Re_\tau = 551$ (details in Huang *et al.* (2026, to appear)). The temporal velocity signal is sectioned, using a Hann window, into 5 temporal segments each with 50% overlap. We determine all small-scale modes that are resonant with L and have mean critical layers at $y^+ = \{2, 32, 270, 424, 500\}$ (Coimbra and McKeon, under review). We only consider triads where L is the largest scale, meaning the spatial wavenumbers of α and β are larger than that of L. Considering the energy transfer of L with modes larger than itself could be an interesting future study. However, there are very few triadic interactions where L is not the largest scale—only a self-interaction of $k_x = 0.5$ would yield $k_{xL} = 1$, and there are many more $|k_z| > 7$ than $|k_z| < 7$. The senses of the net transfers of energy between the small-scale modes and the large scale, N_L, for a single temporal segment are shown by the global cascade arrows (double-lined arrows)

Fig. 2(c). The senses of the net energy transfer between the two small scales, $S(\alpha,L,\beta)$ or $S(\beta,L,\alpha)$, are shown by the local cascades, illustrated by the single-lined arrows. In addition to the spectral interpretation of the cascade, the global and local STS cascades are associated with wall-normal transports of energy, as illustrated.

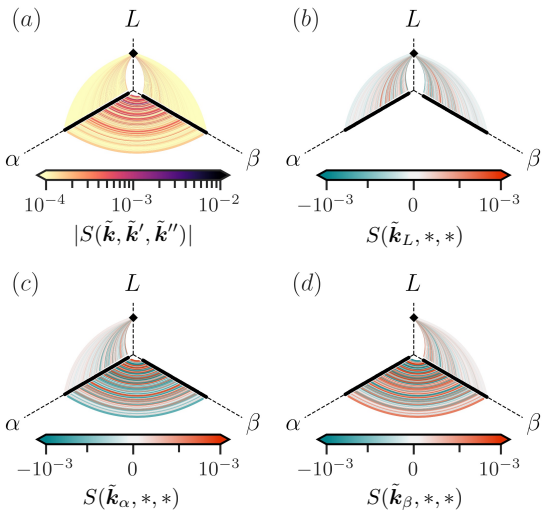

Figure 3. Energy transfer diagrams. (a) The magnitude of the energy transferred along each pathway—the sense of the transfer is obscured. (b) The energy transfer to L from either α or β, noted as $S(\tilde{\boldsymbol{k}}_L,*,*)$ in the color bar label. The left sector shows the energy transferred to L from α, facilitated by β, i.e. $S(\tilde{\boldsymbol{k}}_L,\tilde{\boldsymbol{k}}_\beta,\tilde{\boldsymbol{k}}_\alpha)$. The right sector shows the energy transferred to L from β via α, i.e. $S(\tilde{\boldsymbol{k}}_L,\tilde{\boldsymbol{k}}_\alpha,\tilde{\boldsymbol{k}}_\beta)$. ($c$) Energy transfer to α. The left sector shows $S(\tilde{\boldsymbol{k}}_\alpha,\tilde{\boldsymbol{k}}_\beta,\tilde{\boldsymbol{k}}_L)$ and the bottom shows $S(\tilde{\boldsymbol{k}}_\alpha,\tilde{\boldsymbol{k}}_L,\tilde{\boldsymbol{k}}_\beta)$. ($d$) Energy transfer to β. The bottom and right sectors show $S(\tilde{\boldsymbol{k}}_\beta,\tilde{\boldsymbol{k}}_L,\tilde{\boldsymbol{k}}_\alpha)$ and $S(\tilde{\boldsymbol{k}}_\beta,\tilde{\boldsymbol{k}}_\alpha,\tilde{\boldsymbol{k}}_L)$, respectively.

The individual energy transfer pathways that contribute to the STS cascades are shown in Fig. 3 for the case where the critical layers of α and β have a mean wall-normal location of $y^+ = 32$. For example, in Fig. 3(a), the arcs connecting the α and L axes denote the magnitude of the energy passing between α and L, facilitated by β in the triad, i.e. $|S(\tilde{\boldsymbol{k}}_\alpha,\tilde{\boldsymbol{k}}_\beta,\tilde{\boldsymbol{k}}_L)| = |S(\tilde{\boldsymbol{k}}_L,\tilde{\boldsymbol{k}}_\beta,\tilde{\boldsymbol{k}}_\alpha)|$. Each arc corresponds to the energy transferred in one triad, and the point of intersection on the axes relates to the mode's k_z value. Accordingly, all arcs connecting to the L axis connect at a single point since we consider a single representative L. Arcs near the origin are α and β modes with smaller k_z, and further from the origin are smaller scales, so larger k_z. Figure 3(a) shows the magnitude of the energy exchanged along each pathway, and Figs. 3(b)–(d) show the signed energy transfer relative to L, α, and β, respectively. For example, the bottom sector of Fig. 3(c), shows $S(\alpha,L,\beta)$, i.e. the energy transferred to α from β via L; α,β, and L can sometimes be referred to as the recipient, donor (or source), and advective modes, respectively (e.g. Smyth 1994; Ding *et al.* 2025; Symon *et al.* 2021). The equivalent sector in Fig. 3(d) shows $S(\beta,L,\alpha) = -S(\alpha,L,\beta)$. The sign of the transfer denotes whether the mode gained or lost energy along that pathway. Positive transfer, S, means the mode gained energy (shown in red) and negative transfer means the mode lost energy along that path (shown in blue).

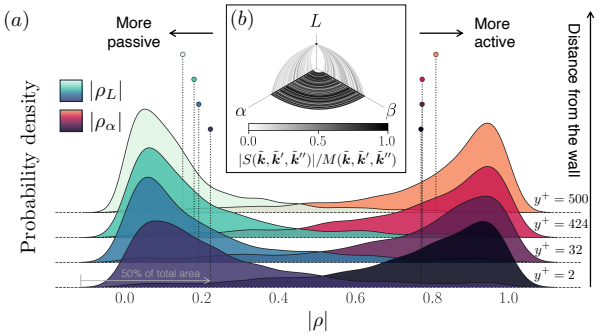

Figure 4. (a) The probability density for the magnitude of the transfer density to L is shown in the blue shades, which all peak closer to 0. In contrast, probability density for the magnitude of the transfer density to α, shown in the red shades, peak closer to 1. The markers indicate the $|\rho|$ at which 50% of the total area under the curve is captured. (b) The magnitude of the energy transferred along each pathway, normalized by the total energy exchanged in the triad, $M(\tilde{\boldsymbol{k}},\tilde{\boldsymbol{k}}',\tilde{\boldsymbol{k}}'')$. Figure 4(b) is Fig. 3($a$) normalized by $M(\tilde{\boldsymbol{k}},\tilde{\boldsymbol{k}}',\tilde{\boldsymbol{k}}'')$.

The bottom sectors in Fig. 3(b) and (c) are therefore equal and opposite. Consequently, the net transfer to a mode $\tilde{\boldsymbol{k}}$ accounts for the transfer to $\tilde{\boldsymbol{k}}$ from the two possible pathways, as defined by $N_{\tilde{\boldsymbol{k}}}$ in eq. 7. It is apparent that the pathways connecting the small-scale modes to L generally transfer less energy than the pathways connecting α and β, indicating that the local STS cascades are the primary pathways for energy transfer. The global STS cascades are still relevant, as there are some interactions where there is more energy transferred in the global cascade, and recall that the global cascade allows for the largest wall-normal transports of energy. For this reason, the global cascades are increasingly relevant for large-scale modes with significant wall-normal extents, such as VLSMs.

It is expected that the net transfer of energy is tied to the magnitude of the wavenumbers in the interactions; from observing power spectra it is known that larger scales tend to contain more energy than smaller scales, so it could be expected that triads involving larger scales have larger quantities of energy to exchange. This is supported qualitatively in Fig. 3(a), where the pathways near the origin (corresponding to larger scales) exchange more energy than at the smaller scales (plotted further from the origin). To better isolate the energy transfer behavior of each mode in the triad relative to other triads with different wavenumbers, the energy transferred along each pathway can be normalized by the total energy being exchanged in the triad,

$$M(\tilde{\boldsymbol{k}},\tilde{\boldsymbol{k}}',\tilde{\boldsymbol{k}}'') = |S(\tilde{\boldsymbol{k}},\tilde{\boldsymbol{k}}',\tilde{\boldsymbol{k}}'')| + |S(\tilde{\boldsymbol{k}}',\tilde{\boldsymbol{k}}'',\tilde{\boldsymbol{k}})| + |S(\tilde{\boldsymbol{k}}'',\tilde{\boldsymbol{k}}',\tilde{\boldsymbol{k}})|. \quad (8)$$

Note that $M(\tilde{\boldsymbol{k}},\tilde{\boldsymbol{k}}',\tilde{\boldsymbol{k}}'')$ is uniquely defined for each triad. The magnitude of the energy transferred by each pathway (Fig. 3(a)) normalized by the total energy exchanged in the triad, $M(\tilde{\boldsymbol{k}},\tilde{\boldsymbol{k}}',\tilde{\boldsymbol{k}}'')$, is shown in the inset of Fig. 4. Upon normalizing for the difference in the total energy exchanged in various triads, we see that the general behavior of energy transfer along each transfer pathway is similar across triads. The net transfer density can be defined as

$$\rho_{\tilde{\boldsymbol{k}}} = \frac{N_{\tilde{\boldsymbol{k}}}}{M(\tilde{\boldsymbol{k}},\tilde{\boldsymbol{k}}',\tilde{\boldsymbol{k}}'')}. \quad (9)$$

Here, $\rho_{\tilde{\boldsymbol{k}}}$ is the net transfer density associated with $\tilde{\boldsymbol{k}}$ in the triad defined by $\tilde{\boldsymbol{k}} = \tilde{\boldsymbol{k}}' + \tilde{\boldsymbol{k}}''$. However, the transfer density for the other two modes in the triad can be equivalently defined by replacing the numerator of eq. 9 with $N_{\tilde{\boldsymbol{k}}'}$ or $N_{\tilde{\boldsymbol{k}}''}$. The probability density for the value for $|\rho_L|$ and $|\rho_\alpha|$ is shown for triads with small-scale critical layers at $y^+ = \{2, 32, 424, 500\}$ in Fig. 4(a). $|\rho_L|$ and $|\rho_\alpha|$ are shown in the blue and red shades, respectively. The behavior for β is qualitatively similar to that of α so is not shown. The markers denote the location at which 50% of the area under the curve is reached. As distance from the wall increases, the peak in the probability density of $|\rho_L|$ shifts closer to 0, while the peak for $|\rho_\alpha|$ shifts towards 1, indicating that L becomes more passive in the energy transfer process, while the small-scales become more active. Here, "passive" and "active" refer to the mode's level of contribution to net energy distribution; if net transfer to a mode was 0, it did not retain (or give) significant energy from (or to) other scales, and was therefore passive. We emphasize here that L is the same across all triads considered, so the STS framework allows us to consider precisely how L exchanges energy with resonant triads at different wall-normal regions of the flow. While L remains passive at all heights, near the wall, L is more active in the energy exchange than in the regions far from the wall.

Spectral cascade among phase-locked triads

In previous sections, we considered the energy transfer within triads with critical layers at different wall-normal locations for a single temporal segment. For these triads, there was always wall-normal transport of energy associated with the spectral transfer of energy. We now consider the case where all three modes in the triad share the same critical layer and thus there is no spatial transport of energy. In this case, the cascade is purely spectral and the fact that all three modes share the same critical layer means that they share the same wave speed, making them phase-locked with each other. Additionally, because $\omega = ck_x$ and all triads with the same critical layer share the same wave speed, if the triadic resonance condition is satisfied on k_x, resonance on ω is automatically satisfied. This effectively reduces the dimensionality of the resonance constraint and, as a result, the number of resonant triads at the same critical layer is very high compared to the number of triads that are at any other given height. As was also mentioned previously, the critical layer of L separates the triads that are interacting and exchanging energy below the critical layer of L and those above the critical layer. Among triads that are resonant with L, energy from below the critical layer can, at most, be transported up to the critical layer of L via a global cascade and can only be moved above the critical layer of L through another triadic interaction with L. For these reasons, we study the energy transfer behavior of these phase-locked modes.

We consider trends in the net transfer to L and the total exchange of energy with L as a function of the magnitude of the mean small-scale wavenumber:

$$\kappa_x = \frac{|k_{x\alpha}| + |k_{x\beta}|}{2}, \quad \kappa_z = \frac{|k_{z\alpha}| + |k_{z\beta}|}{2}. \tag{10}$$

Since the wavenumber for L is fixed, and all modes share the same wave speed, $\boldsymbol{\kappa} = [\kappa_x, \kappa_z]$ uniquely defines a phase-locked triad. The total exchange with L is defined as

$$T_L = |S(\tilde{\boldsymbol{k}}_L, \tilde{\boldsymbol{k}}_\alpha, \tilde{\boldsymbol{k}}_\beta)| + |S(\tilde{\boldsymbol{k}}_L, \tilde{\boldsymbol{k}}_\beta, \tilde{\boldsymbol{k}}_\alpha)|, \tag{11}$$

and is the magnitude of the total energy exchanged along the two pathways involving L, i.e. the pathways shown in the top two sectors of Fig. 3(a). While N_L describes how much energy results in a net transfer to L, T_L describes how much energy is being exchanged with L. A large discrepancy between N_L and T_L would indicate that the energy transfer process is inefficient—a lot of energy is being exchanged across scales, but very little results in a net distribution.

Figure 5(a) and (b) show trends in the net transfer and total exchange with L as a function of κ_x. The κ_x values are grouped bins of width $\Delta\kappa_x = 4$ and the net transfer to L is summed over all κ_x in each bin, denoted κ_x^j, and all κ_z, i.e. $\sum_{i|\kappa_x^j,\kappa_z} N_L^i$. The net transfer is computed for each temporal segment then ensemble-averaged. The standard error (S.E.) and 95% confidence interval (C.I.) associated with the variation across the five ensembles is shown by the filled-in cyan region and vertical grey lines, respectively. Similarly, the total exchange with L is computed by summing the contributions from each κ_x^j bin and all κ_z, shown in Fig. 5(b). Figures 5(c) and (d) show the net transfer and total exchange with L, respectively, as a function of κ_z^j bins rather than κ_x^j. The κ_z bin width is $\Delta\kappa_z = 15$. The insets in Figs. 5(b) and (d) show the total exchange plotted on a semi-log plot. The red dashed lines are an exponential fit, indicating that the total exchange with L decays nearly exponentially with κ_x and κ_z.

First, we note that while the uncertainty across ensembles is higher for low-wavenumbers, at high wavenumbers, the net transfer to L goes to 0 with very low uncertainty. The total exchange is also captured at higher wavenumbers with high confidence levels. Additionally, the magnitude of the net transfer to L is significantly lower than the total amount of energy exchanged with L, and this is particularly notable at the lower wavenumbers. The discrepancy between the net transfer and total exchange indicates that there is significant energy being exchanged with L, but very little is retained by L, making the process of distributing energy across scales quite inefficient.

CONCLUSIONS

The STS framework allows us to incorporate the temporal information from a turbulent channel flow to describe the wall-normal transport of energy associated with the spectral transfer among nonlinear interactions. The estimated spatiotemporal modes that result from taking the Fourier transform of a windowed temporal signal are shown to exactly retain triad-by-triad energy conservation properties. By enforcing triadic resonance on the frequency component of the spatiotemporal wavenumbers, we show that the STS framework admits a symmetric spatial arrangement of resonant modes about the critical layer of the largest scale in the triad. These spatial constraints result in a spatiotemporal-spectral description of the energy cascade that expands the classical description of the energy cascade to include wall-normal transport of energy. The STS cascade can be further split into a global and local cascade: the global STS cascade describes spectrally non-local and spatially expansive transfers of energy while the local STS cascade captures spectrally and spatially local transfers. By considering interactions of a representative VLSM, L, with small-scales at various wall-normal locations, we see that L becomes more passive in the energy exchange process with distance from the wall. At the critical layer of L, there is purely spectral energy transfer among triads where all resonant modes are phase-locked. We computed the net transfer and total exchange with L as a function of the mean small-scale wavenumber magnitude. The total amount of energy traversing the path-

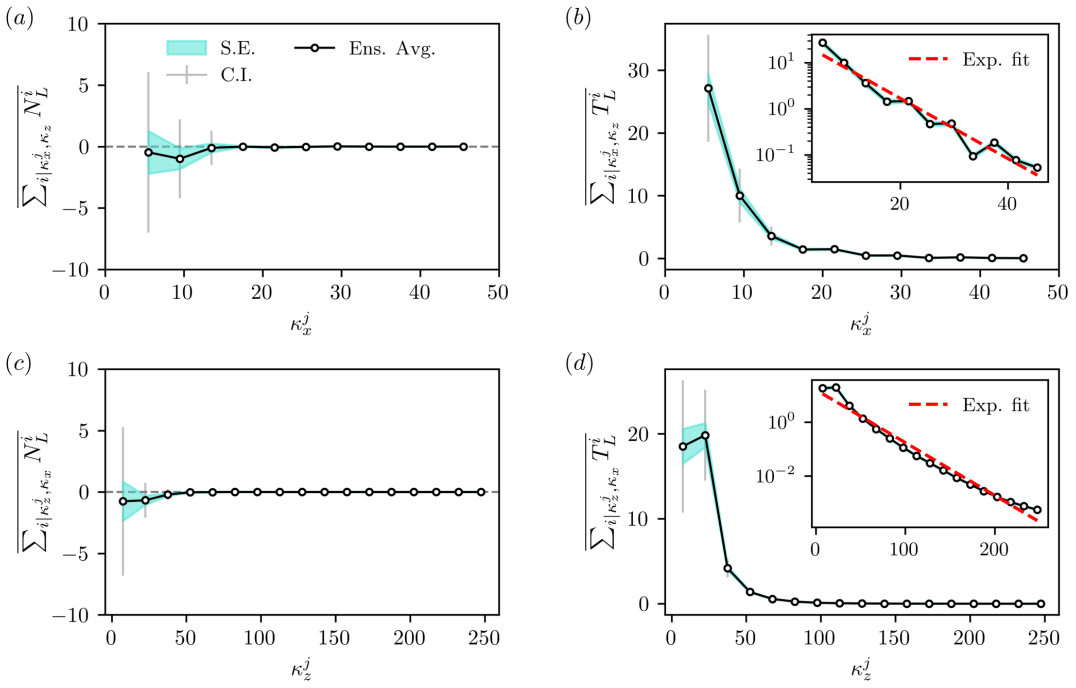

Figure 5. The ensemble-averaged net transfer and total exchange with L as a function of the magnitude of the mean small-scale wavenumber are shown by the black circles. The standard error (S.E.) associated with the variation across the 5 ensembles is shown in the filled cyan region, and the corresponding 95% confidence intervals (C.I.) are shown by the vertical grey lines. (a) The net transfer to L from all κ_z and κ_x in each κ_x^j bin. (b) The total exchange with L from all κ_z and each κ_x^j bin. (c) The net transfer to L from all κ_x and each κ_z^j bin. (d) The total exchange with L from all κ_x and each κ_z^j bin. The insets in (c) and (d) show the total exchange plotted on a semi-log plot with an exponential fit.

ways that connect the small scales with L was shown to decay exponentially with small-scale wavenumber. There was a notable discrepancy in the magnitudes of the net transfer and total exchange of energy with L, indicating that the process of redistributing energy to L from smaller scales is quite inefficient. Ultimately, the STS framework allows us to precisely interrogate the mode-by-mode energy redistribution and transport mechanisms to determine the role of individual modes in energy-exchanging resonant triads. Triadic energy transfer in terms of spatial modes has been the topic of previous studies (e.g. Cho *et al*. 2018; Ding *et al*. 2025) and it would be interesting to reconcile the spatial and spatiotemporal approaches in a future work. In doing so, we can begin to better understand the energetic roles of observed coherent structures in sustaining wall turbulence.

REFERENCES

Barthel, B., 2022, On the variational principles of linear and nonlinear resolvent analysis. PhD thesis, California Institute of Technology.

Cho, M., Hwang, Y. & Choi, H., 2018, Scale interactions and spectral energy transfer in turbulent channel flow. *Journal of Fluid Mechanics* **854**, 474–504.

Coimbra, M. C. Y. & McKeon, B. J., 2024 Permitted spatiotemporal triadic interactions in a turbulent channel. Annual Research Brief. Center for Turbulence Research, Stanford University.

Coimbra, M. C. Y. & McKeon, B. J., 2025 A detailed derivation of energy conservation within a triadic set of spatiotemporal modes. Annual Research Brief. Center for Turbulence Research, Stanford University.

Coimbra, M. C. Y. & McKeon, B. J., 2026, Spatiotemporal architecture of energy transfer in wall-bounded turbulence. Under review.

Ding, J., Chung, J. & Illingworth, S. J., 2025, Mode-to-mode nonlinear energy transfer in turbulent channel flows. *Journal of Fluid Mechanics* **1002**, A42.

Domaradzki, J. A., Liu, W., Härtel, C. & Kleiser, L., 1994, Energy transfer in numerically simulated wall-bounded turbulent flows. *Physics of Fluids* **6** (4), 1583–1599.

Huang, Y., Toedtli, S. S., Chini, G. P. & McKeon, B. J., 2026, Spatio-temporal characterization of nonlinear forcing and response in turbulent channel flow. *Journal of Fluid Mechanics* (to appear).

Jacobi, I., Chung, D., Duvvuri, S. & McKeon, B. J., 2021, Interactions between scales in wall turbulence: phase relationships, amplitude modulation and the importance of critical layers. *Journal of Fluid Mechanics* **914**, A7.

Kraichnan, R. H., 1957, Relation of fourth-order to second-order moments in stationary isotropic turbulence. *Physical Review* **107** (6), 1485–1490.

McKeon, B. J. & Sharma, A. S., 2010, A critical-layer framework for turbulent pipe flow. *Journal of Fluid Mechanics* **658**, 336–382.

Schmid, P. J. & Henningson, D. S., 2001, *Stability and Transition in Shear Flows*, *Applied Mathematical Sciences*, vol. 142. New York, NY: Springer.

Smyth, W. D., 1992, Spectral transfers in two-dimensional anisotropic flow. *Physics of Fluids A: Fluid Dynamics* **4** (2), 340–349.

Symon, S., Illingworth, S. J. & Marusic, I., 2021, Energy transfer in turbulent channel flows and implications for resolvent modelling. *Journal of Fluid Mechanics* **911**, A3.